VISIBLE AND INFRARED REMOTE SENSING

The earliest satellite remote sensing information was supplied by video-style cameras on polar-orbiting satellites. Measuring an integral over a wide range of visible wavelengths, these cameras provided a new perspective to the study of the Earth, making it possible to view features from space that had previously been studied only from the Earth's surface itself. One of the most obvious applications of these satellite data was monitoring clouds and their motion as indicators of changes in weather patterns. This application to meteorology was in fact the primary driving force in the early development of satellite remote sensing. As we matured from polar-orbiting to geostationary satellites our ability to monitor atmospheric conditions improved greatly, resulting in modern systems that give us very high-resolution images of atmospheric pattern changes in time and space. Early (1960s) weather satellites were spin stabilized with their axis and camera pointed at the Earth over the United States, meaning that the satellite could view the Earth only at the latitudes of North America. Today almost everyone on the Earth is accustomed to seeing frequent satellite images collected by geostationary satellites as part of their local weather forecast. This is a very dramatic change that has taken place in slightly over 30 years.

As the meteorological satellites improved it became apparent that satellite data were useful for a great many other disciplines. Some of these other applications used data from the meteorological satellites directly while others awaited new sensors and satellite systems. During those developmental times the National Space and Aeronautics Administration (*NASA*) sponsored the NIMBUS program where a common satellite "bus" was used to carry into space various instruments requiring testing and evaluation. This excellent program ran for about 20 years and was amazingly successful in flying and demonstrating the capabilities of a variety of sensors. One of the greatest successes was the start of the land surface remote sensing satellite series, known as the LANDSAT series. The first few of these starting in 1972 actually used the NIMBUS platform as the spacecraft. Starting with LANDSAT-4 and -5 a new bus was built just for this satellite series. The operation of LANDSAT was privatized in 1980s, and unfortunately the privately developed LANDSAT-6 failed upon launch. LANDSAT-7 was planned to launch in 1998; once again a NASA satellite will usher in a new phase in the study of land surface remote sensing images. Land surface sensing satellites have not been exclusively American. Also designed to measure over the same wavelengths as LANDSAT was the French Système Pour l'Observation de la Terre (*SPOT*) satellite system. The series began with the operation of SPOT-1 on February 22, 1986, and continues today. Companies have been set up to process and sell the SPOT satellite data products.

DEVELOPMENT OF METEOROLOGICAL SATELLITES

NASA's Television Infrared Observation Satellite (*TIROS*-1) (1), launched on 1 April 1960, gave us our first systematic images of Earth from space. This single television camera was aligned with the axis of this spin-stabilized satellite, which meant that it could point at the Earth only for a limited time each orbit (which naturally collected pictures for the latitudes of North America). This experimental satellite series eventually carried a variety of sensors, evolving as technology and experience increased. Working together, NASA and the Environmental Science Services Administration (*ESSA*), merged into the National Oceanographic and Atmospheric Administration (*NOAA*) at the latter's formation in 1970, stimulated improved designs. TIROS-1 through TIROS-X contained simple television cameras, while four of the ten satellites also included infrared sensors.

One interesting development was the change in location of the camera from the spin axis of the satellite to pointing outward from this central axis. The satellite axis was also turned 90° so that now its side, rather than the central axis, pointed toward the Earth. Called the "wheel" satellite, this new arrangement allowed the camera to collect a series of circular images of the Earth, which when mosaicked together provided the first global view of the Earth's weather systems from space.

Using this wheel concept, cooperation between NASA and ESSA initiated the TIROS Operational System (*TOS*) with its first launch in 1966. Odd-numbered satellites carried improved Vidicon cameras and data storage/replay systems that provided global meteorological data, even-numbered satellites provided direct readout Automatic Picture Transmission (*APT*) video to low-cost VHF receiving stations. APT, now derived from Advanced Very High Resolution Radiometry (AVHRR) imagery, is still provided to thousands of simple stations in schools, on ships, and elsewhere worldwide. Nine wheel satellites, called ESSA-1 through ESSA-9, were launched between 1966 and 1969.

The 1970s saw the Improved TOS (*ITOS*), which combined APT and global data collection/recording in each satellite. The major improvement was the use of guidance systems developed for ballistic missiles, which made it possible to stabilize the three axes of the spacecraft. Thus a single camera could be aimed at the Earth, eliminating the need to assemble a series of circular images to map the world's weather. ITOS also introduced day/night acquisitions and a new series of Scanning Radiometers (*SR*s), which offered vastly improved data. Later, ITOS carried the Very High Resolution Radiometer (*VHRR*). As part of international weather data exchange, NOAA introduced the direct reception of VHRR data at no charge to ground stations built by an increasing number of users, beginning in 1972. ITOS-1 and NOAA-1, launched in 1970, were transition satellites of the ITOS series, whereas NOAA-2 through NOAA-5, launched in 1972–1976, carried the VHRR instrument.

The latest generation of this series has been operational since 1978. TIROS-N (for TIROS-NOAA) and NOAA-7 through the latest NOAA-12/NOAA-14, include the AVHRR, discussed in the following section. The major advance introduced with this satellite series was the shift from an analog data relay to a fully digital system. Now the data are digitized onboard the spacecraft before being transmitted to Earth. Also the size and weight of the satel-

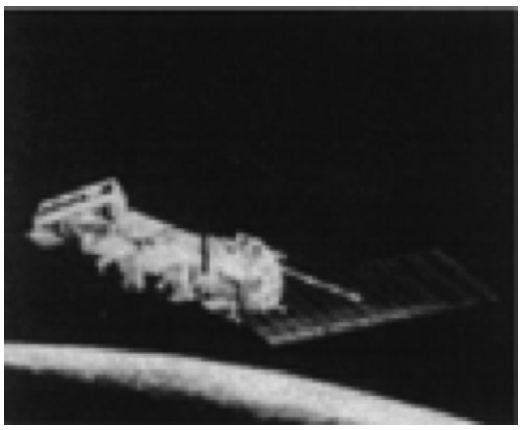

Figure 1. Advanced TIROS-N satellite.

lite has changed from under 300 kg with the ESSA series of satellites to over 1200 kg with the TIROS-N satellites. There has been one change in the TIROS-N series, and we now have the advanced A-TIROS-N, shown in Fig. 1, along with the advanced A-AVHRR or the AVHRR-2. The primary difference in the AVHRR is the addition of a second thermal infrared band to help in the correction for water vapor attenuation when computing sea surface temperature.

The two polar orbiters flying at the time this was first written were NOAA-12 (morning orbit) and NOAA-14 (afternoon orbit). Usually the even-numbered satellites fly in the morning and the odd numbered satellites fly in the afternoon. Because of the premature failure of NOAA-13 it was necessary to put NOAA-14 in the afternoon orbit. A comparison between NOAA-12 and NOAA-14 is given in Table 1. We are now (2006) flying NOAA 18 with one satellite (NOAA-N') left to be launched in this series.

Table 1. Main Characteristics of NOAA-12and NOAA-14

Dimensions	Module type with deployable solar paddle (one wing)
Main Body	3.71 m long, 1.88 m diameter (NOAA-12) 4.18 m long, 1.88 m diameter (NOAA-14)
Solar Array	2.37 m × 4.91 m, 11.6 m^2
Weight	1418 kg at lift-off, 735 kg on orbit (NOAA-12) 1712 kg at lift-off, 1030 kg on orbit (NOAA-14)
Attitude Control	Three-axis stabilized
Design life	Greater than 2 years
Launch Vehicle	ATLAS-E (NOAA-12 Fairing: 6.86 m long, 2.13 m diameter) (NOAA-14 Fairing: 7.42 m long, 2.13 m diameter)
Launch Site	Vandenberg AFB, California
Launch Date	NOAA-12: May 14, 1991; NOAA-14: December 30, 1994
Orbit Type	Sun Synchronous
Approximate Parameters	
Altitude	833 km morning (NOAA-12) 870 km afternoon (NOAA-14)
Inclination	98.7° (NOAA-12); 98.86° (NOAA-14)
Period	101.35 min (NOAA-12); 102.12 min (NOAA-14)
Local time at descending node	0730 a.m. (NOAA-12) 0140 a.m. (NOAA-14)
Sensors	Advanced Very High Resolution Radiometer TIROS Operational Vertical Sounder System (TOVS) Stratospheric Sounding Unit (SSU) High Resolution Infrared Radiation Sounder (HIRS/2) Microwave Sounding Unit (MSU) Space Environment Monitor (SEM) Search and Rescue (SAR) Instruments ARGOS/Data Collection System (DCS)

THE AVHRR

Throughout the developmental process, NOAA has followed a philosophy of meeting operational requirements with instruments whose potential has been proven in space. Predecessor instruments were flown experimentally on experimental satellites before they were accepted and implemented on operational monitoring satellites. These instruments were redesigned to meet both the scientific and technical requirements of the mission; the goal of the redesign was to improve the reliability of the instrument and the quality of the data without changing the previously proven measurement concepts (2). This philosophy brings both benefits and challenges to the user. Benefits revolve around relative reliability, conservative technology, continuity of access, and application of the data compared with other satellite systems. Challenges include desires to use the system beyond its original design, which could have been advanced more rapidly (but at considerably more cost and/or risk of loss of continuity of data characteristics). Challenges also include conflicting desires by users for greater support for their own particular scientific disciplines with more advanced sensors and more sophisticated customer support (while often also desiring even lower-cost imagery) from NOAA.

AVHRR's ancestors were the Scanning Radiometers (*SR*s), first orbited on ITOS-1 in 1970. These early SRs had a relatively low spatial resolution (8 km) and fairly low radiometric fidelity. The VHRR was the first improvement over the SR and for a while flew simultaneously with the SR. Later the VHRR was replaced by the AVHRR which combined the high resolution and monitoring functions. There are two series of AVHRR instruments. Built by ITT Aerospace/Optical Division in the mid-1970s, the AVHRR/1 is a four-channel, filter-wheel spectrometer/radiometer while the AVHRR-2, built in the early 1980s, is identical except for the addition of a second longwave channel (5). The AVHRR instrument is made up of five modules: the scanner module, the electronics module, the radiant cooler, the optical system, and the base plate. Schwalb (3, 4) and ITT (5) provide detailed descriptions of AVHRR hardware.

Starting in Nov. of 1998 a new version called the AVHRR3 (Table 2) was launched on NOAA-15. In this modification of the sensor the mid-wavelength infrared channel is switched from approximately 1.6 μm during the day back to the previous 3.7 μm at night. Thus, the sensor is switching this channel approximately every 45 min during its 90 min orbit. This switch was introduced to provide new snow and ice detection during the day without a major change in the data downlink format.

AVHRR channels 1 and 2 are calibrated before launch and designed to provide direct, quasi-linear conversion between the 10-bit digital numbers and albedo. In addition,

Table 2. AVHRR3 Channel Characteristics

Band	Wavelength (μm)	Nadir Resol. (km)	Swath Width (km)	Typical Use
Band 1 (VIS)	0.58 to 0.68	1.1	2048	Daytime cloud and surface mapping
Band 2 (NIR)	0.725 to 1.1	1.1	2048	Land-water boundaries
Band 3A (NIR)	0.58 to 1.64	1.1	2048	Snow and ice detection
Band 3B (MIR)	3.55 to 3.93	1.1	2048	Night cloud mapping, sea surface temperature
Band 4 (TIR)	10.3 to 11.3	1.1	2048	Night cloud mapping, sea surface temperature
Band 5 (TIR)	11.5 to 12.5	1.1	2048	Sea surface temperature

the thermal channels are designed and calibrated before launch as well as in space (using the AVHRR as a "blackbody" at a measured temperature and cold space to represent 0 °C) to provide direct, quasi-linear conversion between digital numbers and temperature in degrees Celsius. As the thermal infrared channels were optimized for measuring the skin temperature of the sea surface, their range is approximately −25°C to +49°C for channel 3, −100°C to +57°C for channel 4, and −105°C to +50°C for channel 5 for a typical NOAA 11 scene.

DATA INGEST, PROCESSING, AND DISTRIBUTION

There are four classes of AVHRR data: (1) High Resolution Picture Transmission (*HRPT*) data are full-resolution (1 km) data received directly in real time by ground stations; (2) Global Area Coverage (*GAC*) data are sampled on-board to represent a 4.4 km pixel, allowing daily global coverage to be systematically stored and played back to NOAA ground stations at Wallops Island, Virginia, and Fairbanks, Alaska, and a station operated at Lanion, France, by the Centre National d'Edudes Spatiales (*CNES*); (3) Local Area Coverage (*LAC*) data are 1 km data recorded on-board for later replay to the NOAA ground stations; and (4) Automatic Picture Transmission (*APT*) is an analog derivative of HRPT data transmitted at lower resolution and high power for low-cost VHF ground stations. Kidwell (6) provides a handbook for users of AVHRR data.

Special acquisitions of LAC data may be requested by anyone (7). HRPT, LAC, and GAC data are received by the three stations just mentioned and processed at NOAA facilities in Suitland, Maryland. In addition relatively low-cost, direct-readout stations can be set up to read the continuously broadcast HRPT data. Further information about these data, and about NOAA's on-line cataloging and ordering system, can be obtained from:

National Oceanic and Atmospheric Administration National Environmental Satellite Data and Information Service (NESDIS) National Climatic Data Center (NCDC) Satellite Data Services Division (SDSD) Princeton Executive Square, Suite 100 Washington, DC 20233 Tel: (301) 763-8400 FAX: (301) 763-8443

Users of large quantities of data may be able to obtain them more rapidly from NOAA, by making the appropriate individual arrangements with:

Chief, NOAA/NESDIS Interactive Processing Branch (E/SP22) Room 510, World Weather Building Washington, DC 20233 Tel: (301) 763-8142

NOAA'S COMPREHENSIVE LARGE ARRAY-DATA STEWARDSHIP SYSTEM (CLASS)

What was discussed earlier as the Satellite Active Archive (*SAA*) was subsumed by NOAA's new and comprehensive CLASS system. CLASS is a web-based data archive and distribution system for NOAA's environmental data. It is NOAA's premier online facility for the distribution of NOAA and U.S. Department of Defense (DoD) operational environmental satellite data (Geostationary and Polar (GOES and POES), and DMSP) and derived data products. CLASS is evolving to support additional satellite data streams, such as MetOp, EOS/MODIS, NPP, and NPOESS, and NOAA's in situ environmental sensors, such as NEXRAD, USCRN, COOP/NERON, and oceanographic sensors and buoys, plus geophysical and solar environmental data. CLASS is in its second year of a major 10-year growth program, adding new data sets and functionality to support a broader user base. To learn more about CLASS, please visit their online system at http://www.class.noaa.gov.

CLASS Goals

The CLASS project is being conducted in support of the NESDIS mission to acquire, archive, and disseminate environmental data. NESDIS has been acquiring this data for more than 30 years, from a variety of *in situ* and remote sensing observing systems throughout the National Oceanic and Atmospheric Administration (NOAA) and from a number of its partners. NESDIS foresees significant growth in both the data volume and the user population for this data, and has therefore initiated this effort to evolve current technologies to meet future needs.

The long-term goal for CLASS is the stewardship of all environmental data archived at the NOAA National Data Centers (NNDC). The initial objective for CLASS is to support specifically the following campaigns:

- NOAA and Department of Defense (DoD) Polar-orbiting Operational Environmental Satellites (POES) and Defense Meteorological Satellite Program (DMSP)
- NOAA Geostationary Operational Environmental Satellites (GOES)
- National Aeronautics and Space Administration (NASA) Earth Observing System (EOS) Moderate-resolution Imaging Spectroradiometer (MODIS)
- National Polar-orbiting Operational Environmental Satellite System (NPOESS)
- The NPOESS Preparatory Program (NPP)

- EUMETSAT Meteorological Operational Satellite (Metop) Program
- NOAA NEXt generation weather RADAR (NEXRAD) Program

The development of CLASS is expected to be a long-term, evolutionary process, as current and new campaigns are incorporated into the CLASS architecture. This master project management plan defines project characteristics that are expected to be applicable over the life of the project. However, as conditions change over time, this plan will be updated as necessary to provide current and relevant project management guidance.

The goal of CLASS is to provide a single portal for access to NOAA environmental data, some of which is stored in CLASS and some available from other archives. The major processes required to meet this goal that are in scope for CLASS are:

- Ingest of environmental data from CLASS data providers
- Extraction and recording of metadata describing the data stored in CLASS
- Archiving data
- Browse and search capability to assist users in finding data
- Distribution of CLASS data in response to user request
- Identification and location of environmental data that is not stored within CLASS, and connection with the owning system
- Charging for data, as appropriate (see out of scope note below)
- Operational support processes: 24×7 availability, disaster recovery, help desk/user support

While the capability of charging for media delivery of data is a requirement for CLASS, the development of an e-Commerce system to support financial transactions is out of scope. CLASS will interface with another system, NESDIS e-commerce System (NeS), for financial transactions; definition and implementation of the CLASS side of that interface is in scope for this project.

Location/Organization

CLASS is being developed and operated under the direction of the NESDIS Office of Systems Development, having been under the direction of the NESDIS Chief Information Officer (CIO) during the period 2001—2003 (through Release 2.0).

CLASS is being developed by NOAA and contractor personnel associated with the Office of Systems Development (OSD) at the CLASS-MD site in Suitland, MD and at the CLASS_WV site in Fairmont, WV, the National Climatic Data Center (NCDC) in Asheville, NC, and the National Geophysical Data Center (NGDC) in Boulder, CO.

The operational system is currently located at the NOAA facility in Suitland, MD, with a second operational facility at the NCDC facility in Asheville, NC.

The project management is conducted by the CLASS Project Management Team (CPMT), with representatives from each government and contractor team participating in CLASS development and operations and chaired by the OSD Project Manager. Section 2.2 describes the organizational structure for the CLASS project.

Data

Data stored in CLASS includes the following categories:

- Environmental data ingested and archived by CLASS. Currently this includes data for each of the campaigns listed in Section 1.1, and certain product and in situ data
- Descriptive data received with the environmental data, used to support browsing and searching the CLASS archive
- Descriptive data maintained by CLASS to support searching for data maintained in other (non-CLASS) repositories
- Operational data required to support the general operation of the system that is not related to environmental data (e.g., user information, system parameters)

System Overview

An overview of the CLASS system is shown here in Fig. 2, which is a flow chart for the system.

The system functions are to: ingest satellite data and derived data products, create browse products for user selected products and store them online, create netCDF files from selected product data, store some files in permanent cache and others in temporary cache, and archive all data in robotic system. In terms of user services CLASS is to: set up the user profile, initiate catalog search, view search results: catalog data, browse images, dataset coverage maps, order data, view order status, visualize and download product data netCDF files.

Visualization will be done at the user interface in response to requests for browse images of the selected data set. The primary value of these browse images is to determine if the right area was selected and whether or not an image contains an abundance of cloud cover. The system delivers the URL of the browse image to the user's computer for display.

Once it is determined that the data granule is to be ordered the order is confirmed by the user and the order module locates the data set in terms of data type, time range, geographic range or other criteria. The data files are located in the robotic storage and retrieved for processing. The requested file is generated from the storage file and the requested file is put on temporary cache for user retrieval. The data is kept there for several days. These files can be transferred by standard FTP for future analysis and storage by the users. The system notifies users by email when the data files are ready for transfer. It is possible to regularly subscribe for certain types and amounts of data. Similarly it is possible to "bulk order" data on CLASS.

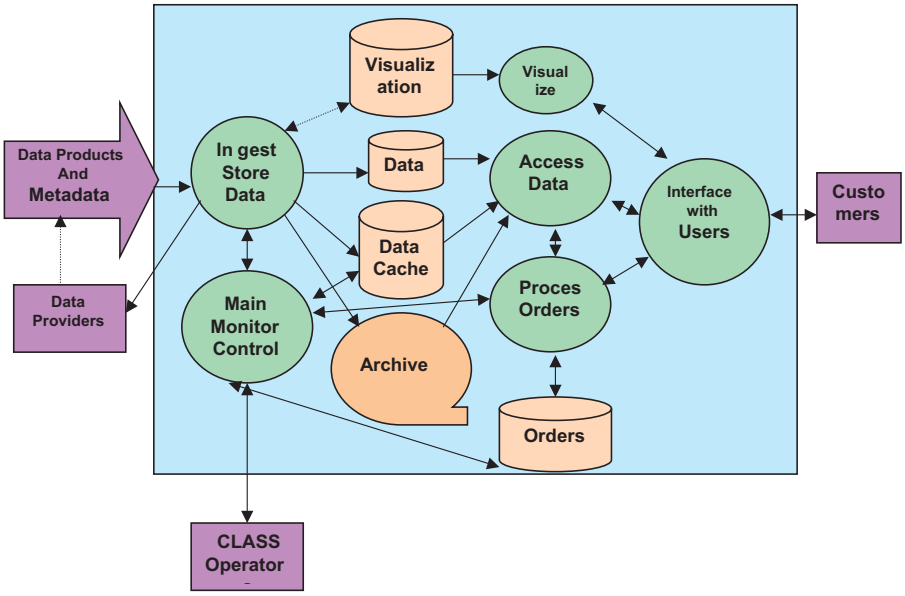

Figure 2. CLASS System Overview Diagram.

The system command unit oversees the operation of CLASS and monitors its activities. There is a backup system to insure continued operation and secure archival of all the data in CLASS.

NATIONAL POLAR-ORBITING OPERATIONAL SATELLITE SYSTEM (NPOESS)

On May 15, 1994 The U.S. President issued a "Decision Directive" that the three separate polar-orbiting satellite programs operated by NOAA, the DoD and NASA should be converged into a single program of polar-orbiting satellites. An Integrated Program Office (IPO) was formed and located in Silver Springs, Md. Which was staffed by NOAA, NASA and DoD personnel contributed by each agency to this joint effort.

Although a NOAA program the procurement of this system followed along DoD lines and representatives of these agencies met and defined a list of Environmental Data Records (EDRs) that the sensors on NPOESS must be able to measure and provide. With each EDR an accuracy, precision were also given by the IPO. The primary sensors were then defined by the IPO and requests for proposals were initiated. The instruments were initially contracted separately by the government. The primary sensor is the Visible/Infrared Imaging Radiometer Suite (VIIRS), which was to take over the functions of the AVHRR in terms of the visible and infrared measurements. In addition VIIRS was to include the bands of NASA's MODerate resolution Imaging Spectrometer (MODIS) that had ocean color bands instead of the broad visible band of the AVHRR.

The NPOESS satellite (Fig. 3) is a relatively large satellite and will carry a number of instruments. There will first be an NPOESS Preparatory Platform (NPP), which is a NASA satellite that will carry three of the future NPOESS instruments. The first will be the VIIRS just mentioned in addition to the Cross-track Infrared Sounder (CrIS) and the Advanced Technology Microwave Sounder (ATMS).

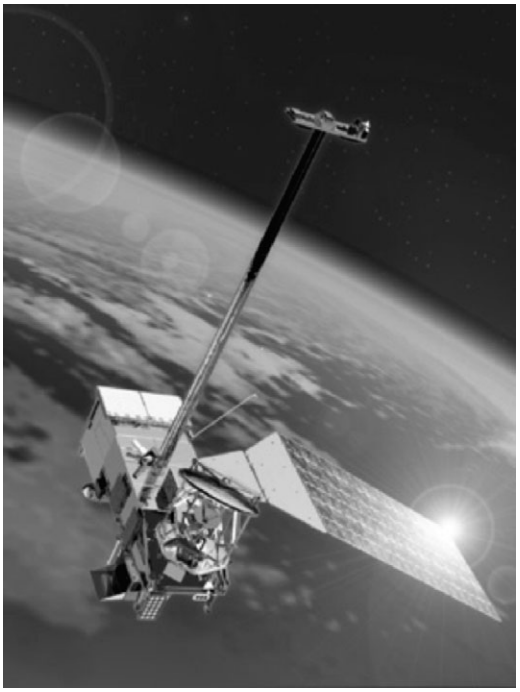

Figure 3. NPOESS satellite.

These latter two instruments exploit the infrared and passive microwave portions of the spectra to profile the lower atmosphere providing information critical for operational weather forecasting.

The VIIRS will have 21 channels ranging from 412 nm to 11450 nm. The visible channels are quite narrow (20 nm) to allow for the computation of ocean color indications of chlorophyll and to accurately sense land surface vegetation. A schematic for the VIIRS instrument is presented here in Fig. 4, which shows the processing of a photon received by the instrument to the end product.

A prime contractor was selected to build the NPOESS satellites and the corresponding ground system. This was awarded to Northrop Grumman together with Raytheon Corp. It was decided to have the prime contractor also handle the administration of the subcontracts to the selected instrument vendors. The VIIRS had been awarded to Raytheon Santa Barbara Research Systems, the CrIS to ITT in Fort Wayne, Indiana and the ATMS to Aerospace Corp., which was later taken over by Northrop Gruman as well.

During its development phase this program dramatically overran its budget and finally hit a boundary where a DoD program was required by congress to undergo a review. This review was agreed to by NOAA and NASA. As a result of this review NPOESS has been dramatically scaled back with the cancellation of some planned instruments and the reduction from three to only two satellites operating at the same time. Also the launch of the first NPOESS satellite was delayed from 2009 to 2012.

NASA'S MODERATE RESOLUTION IMAGING SPECTRORADIOMETER (MODIS)

MODIS was the primary imager selected for NASA's Earth Observing System. Awarded to Raytheon's Santa Barbara lab it became a precursor for the NPOESS VIIRS instrument. First launched on NASA's TERRA satellite on Dec.18, 1999 MODIS began collecting data on Feb. 24, 2000.

The MODIS instrument provides high radiometric sensitivity (12 bit) in 36 spectral bands ranging in wavelength from 0.4 μm to 14.4 μm. The responses are custom tailored to the individual needs of the user community and provide exceptionally low out-of-band response. Two bands are imaged at a nominal resolution of 250 m at nadir, with five bands at 500 m, and the remaining 29 bands at 1 km. A $\pm$55-degree scanning pattern at the EOS orbit of 705 km achieves a 2,330-km swath and provides global coverage every one to two days.

The Scan Mirror Assembly uses a continuously rotating double-sided scan mirror to scan $\pm$55-degrees and is driven by a motor encoder built to operate at 100 percent duty cycle throughout the 6-year instrument design life. The optical system consists of a two-mirror off-axis afocal telescope, which directs energy to four refractive objective assemblies; one for each of the VIS, NIR, SWIR/MWIR and LWIR spectral regions to cover a total spectral range of 0.4 to 14.4 μm. A high-performance passive radiative cooler provides cooling to 83K for the 20 infrared spectral bands on two HgCdTe Focal Plane Assemblies (FPAs). Novel photodiode-silicon readout technology for the visible and near infrared provide unsurpassed quantum efficiency and low-noise readout with exceptional dynamic range. Analog programmable gain and offset and FPA clock and bias electronics are located near the FPAs in two dedicated electronics modules, the Space-viewing Analog Module (SAM) and the Forward-viewing Analog Module (FAM). A third module, the Main Electronics Module (MEM) provides power, control systems, command and telemetry, and calibration electronics. The system also includes four onboard calibrators as well as a view to space: a Solar Diffuser (SD), a v-groove Blackbody (BB), a Spectroradiometric calibration assembly (SRCA), and a Solar Diffuser Stability Monitor (SDSM).

A second MODIS instrument was launched on the AQUA satellite May 4, 2002 giving us both a morning (TERRA) and afternoon (AQUA) Earth viewing with MODIS instruments. The afternoon orbit of AQUA is one in which a whole series of satellites will be operated and it has become known as the A-Train.

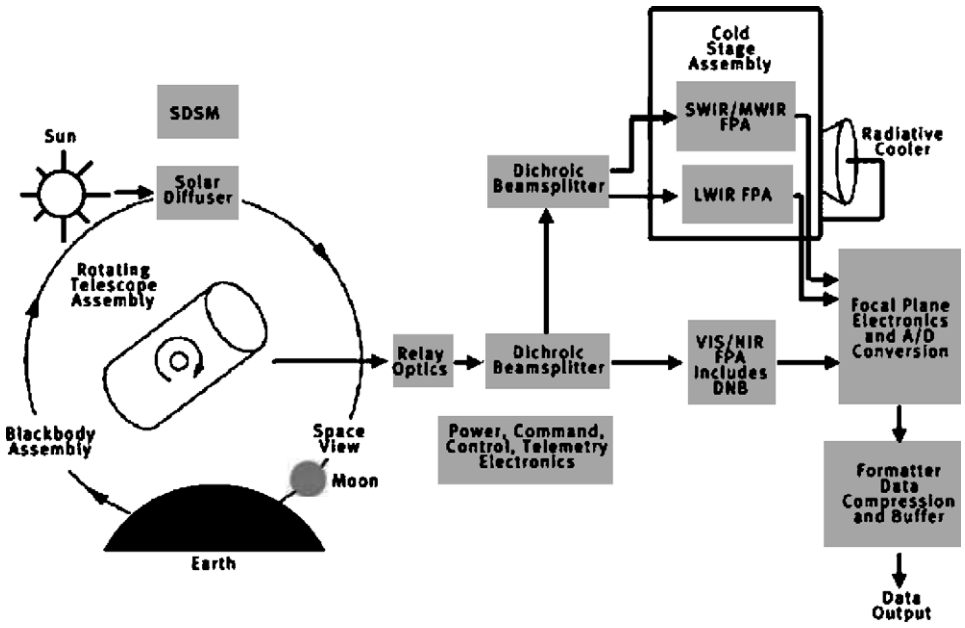

Figure 4. VIIRS schematic operation description.

THE GEOSTATIONARY OBSERVING ENVIRONMENTAL SATELLITE (GOES)

To monitor changes in the atmosphere related to the Earth's weather accurately, it is necessary to sample much more frequently than is possible with a polar-orbiting satellite. Thus geostationary satellite sensors were created to make it possible to sample rapidly from geostationary orbit. The much greater altitudes of geostationary orbits (36,000 km versus 800 km for polar orbits) require much more sensitive instruments than were flown earlier in polar orbit. In addition, because the early geostationary satellites were spin-stabilized, the sensors needed to be able to operate on this spinning satellite. Thus each scan could view the Earth only for a period of time set by the rotation of the spacecraft. The solution came in the form of what was originally called the spin scan camera, which was later called the spin scan radiometer. The key to the success of this unit was that it used the spin of the satellite to mechanically cause the telescope to scan the Earth's surface and also used the satellite's spin to increment the scan mirror vertically. Called the Visible Infrared Spin Scan Radiometer (*VISSR*, Fig. 5), it would scan the surface of the Earth from north to south or vice versa. This basic system continued up to the early 1990s when a new generation of geostationary orbiting environmental satellites (*GOES*) were deployed. Using control systems similar to those used in polar orbiter, the new GOES are three-axis stabilized and maintain their orientation to the Earth (Fig. 6). This orientation makes it possible to "stare" at the Earth, increasing the amount of radiative energy available for Earth surface sensing and so resulting in higher spatial resolutions. This new constant orientation to the Earth also results in a satellite that is constantly heated at one end and cooled at the other. A complex system is required to maintain thermal equilibrium. The GOES Imager (Fig. 7) is a multichannel instrument designed to sense radiant and solar-reflected energy from sampled areas of the Earth. The multielement spectral channels simultaneously sweep east-west and west-east along a north-to-south path by means of a two-axis mirror scan system. The instrument can produce full-Earth disk images, sector images that contain the edges of the Earth, and various sizes of area scans completely enclosed within the Earth scene using a new flexible scan system. Scan selection permits rapid continuous viewing of local areas for monitoring of mesoscale (regional) phenomena and accurate wind determination.

The GOES system produces a large number of primary data products. They include

- Basic day/night cloud imagery and low-level cloud and fog imagery,
- Upper and lower tropospheric water vapor imagery,
- Observations of land surface temperature data with strong diurnal variation,
- Sea surface temperature data,
- Winds from cloud motions at several levels and hourly cloud-top heights and amounts,
- Albedo and infrared radiation flux to space, important for climate monitoring and climate model validation,

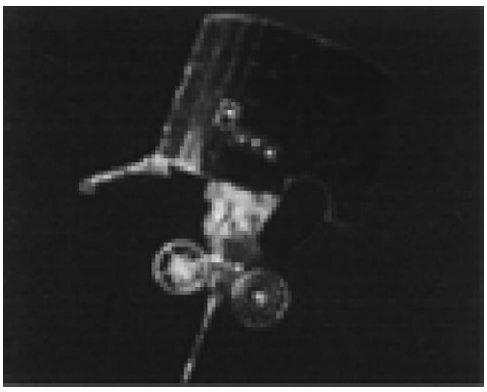

Figure 5. GOES spinner spacecraft.

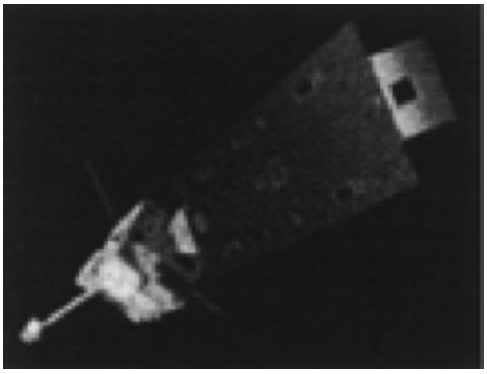

Figure 6. Three-axis stabilized GOES.

- Detection and monitoring of forest fires resulting from natural causes and/or human-made causes and monitoring of smoke plumes,
- Precipitation estimates,
- Total column ozone concentration (potential data product), and
- Relatively accurate estimates of total outgoing longwave radiation flux (potential data product).

These data products are summarized in Table 3.

These data products enable users to monitor severe storms accurately, to determine winds from cloud motion, and, when combined with data from conventional meteorological sensors, to produce improved short-term weather forecasts. The major operational use of 1 km resolution vis-

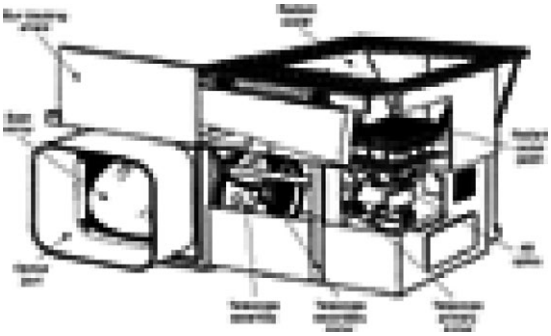

Figure 7. The GOES Imager.

Table 3. Imager Channels and Products

Product	Channel Wavelength (μm)	1 0.65	2* 3.9	3* 6.7	4 11	5* 12
Clouds		x	x	x	x	x
Water vapor*				x	x	x
Surface temp.			o		x	o
Winds		x		x	x	
Albedo + IR flux	x		o	x	o	
Fires + Smoke	x	x		o	o	

KEY: * new operational data.
x primary channel.
o secondary channel.

ible and 4 km resolution infrared multispectral imagery is to provide early warnings of threatening weather. Forecasting the location of probable severe convective storms and the landfall position of tropical cyclones and hurricanes is heavily dependent upon GOES infrared and visible pictures. The quantitative temperature and moisture and wind measurements are useful for isolating areas of potential storm development.

GOES data products are used by a wide variety of both operational and research centers. The National Weather Service's (*NWS*'s) extensive use of multispectral imagery provides early warnings of threatening weather and is central to its weather monitoring and short-term forecast function. Most nations in the western hemisphere depend on GOES imagery for their routine weather forecast functions as well as other regional applications. GOES data products are also used by commercial weather users, universities, the Department of Defense, and the global research community, particularly the International Satellite Cloud Climatology Project, through which the world's cloud cover is monitored for the purpose of detecting change in the Earth's climate. Users of GOES data products are also found in the air and ground traffic control, ship navigation, agriculture, and space services sectors.

The GOES system serves a region covering the central and eastern Pacific Ocean; North, Central, and South America; and the central and western Atlantic Ocean. Pacific coverage includes Hawaii and the Gulf of Alaska. This is accomplished by two satellites, GOES West located at 135° west longitude and GOES East at 75° west longitude. A common ground station, the Central Data Antenna (*CDA*) station located at Wallops, Virginia, supports the interface to both satellites. The NOAA Satellite Operations Control Center (*SOCC*), in Suitland, Maryland, provides spacecraft scheduling, health and safety monitoring, and engineering analyses. Delivery of products involves ground processing of the raw instrument data for radiometric calibration and Earth location information and retransmission to the satellite for relay to the data user community. The processed data are received at the control center and disseminated to the NWS's National Meteorological Center (*NMC*), Camp Springs, Maryland, and NWS forecast offices, including the National Hurricane Center, Miami, Florida, and the National Severe Storms Forecast Center, Kansas City, Missouri. Processed data are also received by Department of Defense installations, universities, and numerous private commercial users. An example infrared (*IR*) image is shown in Fig. 8 for GOES 9 located in the eastern position.

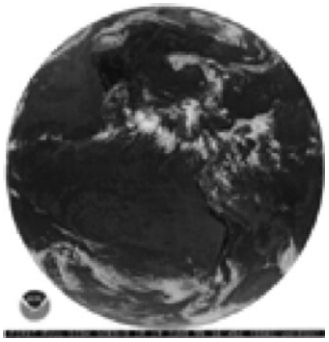

Figure 8. Full disk GOES-9 IR image on June 19, 1995.

GOES Generations

We are now in the second generation of the 3-axis stabilized GOES series of satellites, which will take us into the next decade, and we are planning for their follow on in 2012. This will be the GOES-R program, which will see a dramatic improvement in the capability of the GOES imager. The new Advanced Baseline Imager (ABI) already awarded to ITT will have channels similar to MODIS and the future VIIRS instruments. Even though in geostationary orbit the ABI will have capabilities closer to MODIS including multiple infrared channels and narrow visible channels for ocean color and land surface vegetation studies. In addition the ABI will be able to rapidly scan not only the entire hemisphere that it views but also even more rapidly the central U.S. and even more quickly smaller "mesoscale" regions where the development of severe weather is anticipated.

Recently due to anticipated cost and complexity the future GOES-R sounder known as the Hyperspectral Environmental Sounder (HES) has been cancelled at least for the first couple of GOES-R satellites. Instead there is an expectation that the present generation of GOES sounding instruments will be carried by these satellites.

DEVELOPMENT OF EARTH RESOURCES TECHNOLOGY SATELLITES

The first satellite in the Earth Resources Technology Satellite (*ERTS*) program was launched in 1972 and designated ERTS 1. In 1975 the program was redesigned as the LANDSAT program to emphasize its primary area of interest, land resources. The mission of LANDSAT is to provide for repetitive acquisition of high-resolution multispectral data of the Earth's surface on a global basis. As mentioned earlier, the first three Earth Resources Technology Satellites (*ERTS*-1,2,3) were actually modified NIMBUS satellites with a sensor suite focused on sensing the land surface. These were later referred to as LANDSAT-1, 2, and 3 and all three greatly outlasted their design life of just one year. They carried a four-channel Multispectral Scanner (*MSS*), a three-camera return beam vidicon (*RBV*), a data collection system (*DCS*), and two video tape recorders. The MSS operated over the following spectral intervals: band 4 (0.5 to 0.6 μm), band 5 (0.6 to 0.7 μm), band 6 (0.7 to 0.8 μm), and band 7 (0.8 to 1.1 μm). Three independent cameras,

making up the RBV, covered three spectral bands: blue-green (0.47 to 0.575 μm), yellow-red (0.58 to 0.68 μm), and near-infrared (0.69 to 0.83 μm). Both systems viewed a ground scene of approximately 185 km by 185 km area with a ground resolution of about 80 m. On LANDSAT 1, the RBV was turned off because of a malfunction. LANDSAT-3 added a fifth channel in the thermal infrared (10.4 to 12.6 μm) to the MSS.

The LANDSAT satellites are in a sun-synchronous, near polar orbit with a ground swath extending 185 km (115 mi) in both directions. LANDSAT-4 and -5 were inclined 98° and had an orbital cycle of 16 days and an equatorial crossing of 9:45 A.M. local time. The altitude of the satellites is 705 km (437 mi) for both LANDSAT-4 and -5. Working together, LANDSAT-4 and -5 offer repeat coverage of any location every 8 days. At the equator, the ground track separation is 172 km, with a 7.6% overlap. This overlap gradually increases as the satellites approach the poles, reaching 54% at 60° latitude. The data from both instruments were transmitted directly to a ground receiving station when the satellite was within range. During those periods when the satellite was not in view of a US owned and operated ground station the satellites were only turned on according to a predetermined schedule. The satellite did not carry enough tape recording capacity to record very many of the MSS images, and it thus motivated the international science community to use its global recording capability to download the images from these satellites and make them available to interested parties. This practice led to the establishment of LANDSAT receiving stations all over the world. At present, these stations must pay an annual license fee to EOSAT Corporation in order to receive and use LANDSAT data in their own area of recording coverage.

LANDSAT-4 and -5 were built as specific satellites for their applications dropping the NIMBUS bus along the way. Not only was the spacecraft a new system, but a new scanner also had been developed for these satellites. Called the thematic mapper (*TM*), the instrument was designed to give some very specific signatures for various types of resource related surface features. The TM has seven spectral bands covering four regions of the electromagnetic spectrum: bands 1 to 3 the visible range (0.45 μm to 0.69 μm), band 4 the near-infrared (1.55 μm to 2.35 μm), and the thermal infrared band 7 (10.4 μm to 12.5 μm). There was also a physical difference between the TM and the MSS in that the MSS scanned only in one direction, whereas the TM scanned and collected data in two different directions. Also in the TM, the target energy fell almost directly on the detector face, whereas the MSS energy must travel fiber optics before getting to the detector, making it easier for the TM to sense changes in the target. A summary of all LANDSAT satellites is given in Table 4, which shows that only one satellite is operating in 1997 and then on a reduced scale. The loss of LANDSAT-6 has severely curtailed research efforts with data from these satellites.

Table 4. History of LANDSAT 1 Through 6

Satellite	Launch	Sensor Status	
LANDSAT-1	23/07/72	MSS	End of operation: 06/01/78
LANDSAT-2	22/01/75	MSS	End of operation: 05/02/82
LANDSAT-3	05/03/78	MSS	End of operation: 31/03/83
LANDSAT-4	16/07/82	MSS, TM	Standby since 07/87
LANDSAT-5	01/03/85	MSS, TM	Operational
LANDSAT-6	October 1993	MSS, ETM	Lost

THE FRENCH SPOT SATELLITES

A program also designed to measure in the same wavelength domain as LANDSAT was the French Système Pour l'Observation de la Terre (*SPOT*) satellite system. The series began with the operation of SPOT-1 on February 22, 1986, which carried the multimission platform that could be modified for future payloads. Operational activities of SPOT-1 ceased at the end of 1990, but it was later reactivated on March 20, 1992 and later stopped tracking on August 2, 1993. SPOT-1 was put into a sun-synchronous orbit with a repeat cycle of 26 days (5 days with pointing capability).

The SPOT-1 payload consisted of two High Resolution Visible (HRV) scanners, which were pointable CCD push-broom scanners with off-nadir viewing: $\pm 27°$ (in steps of 0.6°) or 460 km. These scanners can be operated in two modes: multispectral and panchromatic. In the panchromatic mode, the sensor was capable of a 10 m spatial resolution, which in the multispectral domain doubled to 20 m. In both configurations, the swath width was 60 km. The sensor bands were 0.50 μm to 0.59 μm, 0.61 μm to 0.68 μm, 0.79 μm to 0.89 μm, and 0.51 μm to 0.73 μm. This configuration was retained for SPOT-2, which was made operational on January 21, 1990. The next satellite SPOT-3 was launched on September 26, 1993 and made operational on May 24, 1994. On November 13, 1996, the satellite entered the safehold mode and was no longer operational. Since then, SPOT-2 has continued to operate. In 1997 both SPOT-1 and SPOT-2 have operated simultaneously, providing greatly improved coverage. The SPOT-3 payload consisted of two HRVs (same as SPOT-1), *POAM* II (Polar Ozone and Aerosol Measurement), and *DORIS* (Doppler Orbitography and Radio-positioning Integrated by Satellite). As an example of this class of satellites the 2 m $\times$ 2 m $\times$ 4.5 m SPOT-1 weighed 1907 kg and had a solar array system capable of producing 1 kW from a span of 8.14 m. The orbital altitude at the equator was 822 km and the orbital period was 101.4 min. The on-board tape recorders were capable of 22 min of data collection.

The SPOT orbit is sun-synchronous and nearly circular. The altitude is again about 822 km, the inclination is 98°, there are 14 and 5/26 orbits in each Earth day for a repeat cycle of 26 days during which time the satellite has completed 369 orbits. Because the valid comparison of images of a given location acquired on different dates depends on the similarity of the conditions of illumination, the orbital plane must also form a constant angle relative to the sun direction. This is achieved by ensuring that the satellite overflies any given point at the local time, which in turn requires that the orbit be sun-synchronous (descending node at 10:30 A.M.).

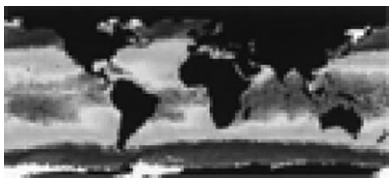

Figure 9. SPOT's stereo viewing capability.

A big change is planned for SPOT-4, which will now carry two HRV Infrared (*HRVIR*) radiometers. The spatial resolutions and swath widths have not changed from earlier systems. The spectral bands are changed slightly and are 0.50 μm to 0.59 μm, 0.61 μm to 0.68 μm, 0.79 μm to 0.89 μm, 1.58 μm to 1.75 μm, and 0.61 μm to 0.68 μm. In addition, SPOT-4 will carry the Vegetation Monitoring Instrument (*VMI*), which has a resolution of 1 km and a swath width of 2,000 km. The sensor bands are 0.43 μm to 0.47 μm, 0.50 μm to 0.59 μm, 0.61 μm to 0.68 μm, 0.79 μm to 0.89 μm, and 1.58 μm to 1.75 μm. A SPOT-5 is planned for late 1999 and will likely carry the same sensor array as does SPOT-4.

One of the unique capabilities of the SPOT series of satellites is their ability to produce stereo imagery for making three-dimensional images of ground subjects. This ability is achieved by being able to point the sensor in a desired direction (Fig. 9). SPOT's oblique viewing capacity makes it possible to produce stereo pairs by combining two images of the same area acquired on different dates and at different angles, due to the parallax thus created. A base/height (B/H) ratio of 1 can be obtained for a viewing angle of 24° to the east and to the west. For a stereo-pair comprising a vertical view and one acquired at 27°, a B/H of 0.5 is obtained. Stereo pairs are mainly used for stereo-plotting, topographic mapping, and automatic stereo-correlation, from which Digital Elevation Models (*DEM*s) can be directly derived without the need for maps.

SPOT satellites can transmit image data to the ground in two ways, depending on whether or not the spacecraft is within range of a receiving station. As the satellite proceeds along its orbit, four situations arise concerning imagery acquisition and image data transmission to ground.

1. The satellite is within range of a Direct Receiving Station (*DRS*), so imagery can be down-linked in real-time provided both satellite and DRS are suitably programmed. The DRS locations are shown in Fig. 10.
2. The satellite is not within range of a SPOT DRS. Programmed acquisitions are executed, and the image data are stored on the on-board recorders.
3. The satellite is within range of a main receiving station (Kiruna or Toulouse). It can thus be programmed either to down-link image data in real-time or play back the on-board recorders and transmit image data recorded earlier during the same orbital revolution.
4. The rest of the time, the satellite is on standby ready to acquire imagery in accordance with uplinked commands.

Figure 10. SPOT Direct Receiving Stations.

Applications of Satellite Imagery

In this section we will present some of the applications of visible, near-infrared, and thermal infrared satellite data. This review of satellite data applications can by no means be comprehensive, and we will instead present examples of the types of applications that can be made with these satellite images. Our review will naturally represent the experience of the author, and it is not intended to neglect other important applications. It is simply easier to present those application most familiar to the author.

Visible and Near-Infrared Applications

Meteorological Applications. The very first use of satellite data was the depiction of changes in cloud patterns that were associated with atmospheric systems. First Earth views were restricted by a spin-stabilized satellite to a limited latitude band. It was increased to daily coverage of the entire Earth as the sensor was oriented to point out from the axis of rotation, which was changed to be perpendicular to the Earth's surface. These global maps were a collage of different synoptic conditions collected over 24 h. Even though these global world views were new and unique, the meteorologists really wanted a time series of their areas of interest, which led to the development of the GOES satellites with their ability to sample a full hemisphere every half hour (Fig. 5). For limited locations, the sampling frequency can be increased to five images every few minutes. Initially the satellite images themselves were the primary sources of information for the weather forecasters. Cloud images were interpreted together with atmospheric pressure maps and some early numerical model results to create the local forecast. The ability to follow the movement of the cloud features in time greatly enhanced the understanding of the evolution of various atmospheric phenomena.

Later a system was developed to profile the atmospheric temperature from geostationary orbit called the VISSR Atmospheric Sounder (*VAS*). Similar to TOVS, the VAS used infrared channels to estimate the atmospheric temperature profiles. The advent of the three-axis stabilized GOES satellites ushered in a new era of atmospheric profiling with the new GOES sounder. These sounding profiles are assimilated into numerical models that do the prediction. Because it is much easier to define the relationship between the numerical models and the satellite's temperature profiles, these are then primary sources of forecast information. The images continue to have value particularly

for the study of poorly understood weather phenomena. The ability to sample rapidly in time has made the new GOES satellites very important for scientific studies that are trying to understand the formation of severe weather and their causes.

Vegetation Mapping. There are many land surface applications that benefit from the combination of near-infrared sensing with visible sensor data. For this reason we treat it together with the purely visible channels which are widely exploited for many different applications. It is not possible to treat each application individually here so we make a few comments about some of the more important applications of these near-infrared data. One of the most popular combinations of AVHRR data uses the visible (0.53 μm to 0.68 μm) channel together with the near-infrared (*NIR*; 0.71 μm to 1.6 μm) to become the Normalized Difference Vegetation Index (*NDVI*) which is defined as

$$\mathrm{NDVI} = \frac{\mathrm{VIS} - \mathrm{NIR}}{\mathrm{STN\,DEV\,(VIS)} - \mathrm{STN\,DEV\,(NIR)}} \qquad (1)$$

This vegetation index combines the visible and near-infrared to form an index that when normalized by the standard deviations ranges between +1 and −1. This index indicates how well the vegetation is growing rather than the amount of biomass present. The visible channel responds to the greening up of the vegetation as it emerges either as a new plant or one that has lain dormant. With SPOT and LANDSAT, it is possible to actually view this change in the green radiation band. For other satellites such as the NOAA-AVHRR, the visible channel is so broad that it covers all the visible wavelengths. We can still use the formulation in Eq. (1) to compute our NDVI because the visible channel is centered in the red. The NIR channel responds to the mesophyll structure in the leaves, which is a function of the amount of water held in the leaves. This is an important sensing mechanism because the leaves will go from brown to green early in the growing season. Later on, their greenness will be saturated, and the leaves will not get any greener. During this time, the leaves will indicate the condition of the plant as they reflect the NIR wavelengths back up to the satellite.

In reality, the NDVI does not really go from −1 to +1 but instead ranges from low negatives up to 0.7 or 0.8. For display on a satellite image, the NDVI must be converted back to a raster image, which requires a scaling from the NDVI value to an 8-bit raster display value (which limits the dynamic range). As an example we present in Fig. 11 the NDVI for the state of Kansas, which is predominantly wheat-growing country. Here we show a series of years all using the same color scale so that changes in color are related to changes in the health of the vegetation. The substantial variability between individual years can clearly be seen even in these small images. Note that the color scale has been created to be brown when the NDVI is low and yellow to red when the vegetation is very healthy. Also the NDVI is never greater than 220 even though it has a theoretical maximum of 255 (the 8 bit equivalent of +1) nor does it go below 120 (−1 would be equal to 0).

These NDVI images have been constructed from a series of daily AVHRR images using channels 1 and 2. Because clouds will obscure the surface in either of these channels, it is necessary to eliminate the cloud cover. This is done in a series of steps. First a cloud classifier or locator program is run to determine which features are clouds. Those pixels clearly defined as clouds are set to a uniform value (usually 0 or 255) in the individual image. The non-cloud pixels of the individual images are composited to construct the single image that covers a number of days. Compositing of the NDVI is done by retaining the maximum value whenever it occurs. This overwrites any values that are not the maximum. Clouds will have the effect of lowering the NDVI so that this type of maximum compositing further reduces the effects of clouds. Realize, however, that even this NDVI composite is not totally free from cloud effects. Clouds that are smaller than the AVHRR pixel size will be brought into this calculation. Here again the NDVI maximum composite will minimize the effects of these sub pixel clouds.

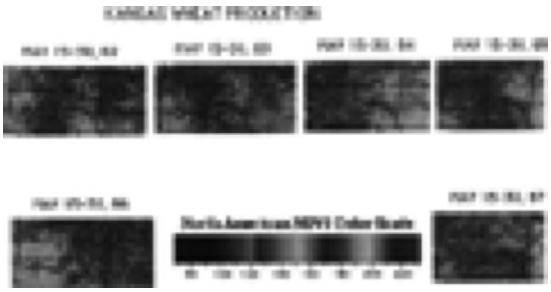

Figure 11. The NDVI for Kansas for 6 years 1982–1987.

Other sources of error in the NDVI calculation are the effects of atmospheric aerosols and possible errors in geolocation of the pixel. The latter very dramatically affects the NDVI particularly in areas of strong inhomogeneity. It is often a difficult problem to detect as the changes will just appear as normal temporal changes in the NDVI. The aerosol influence is also difficult to recognize and is difficult to correct for. There are few direct measurements of atmospheric aerosols to use for correcting the satellite data derived NDVI. Unfortunately, the satellite data technique for estimating aerosols is also based on a combination of the visible and near-infrared channels—the very data that was used to construct the NDVI. Cases where the aerosol effect becomes large are often associated with volcanic eruptions that introduce ash into the upper atmosphere, changing the visible and near-infrared signals. These events can last for weeks and even months depending on the strength and location of the ash plume. Very strong eruptions with a marked ash component have produced ash plumes that have circled the globe before the ash has diffused sufficiently to no longer influence the NDVI computation.

There is considerable discussion on how to interpret the NDVI and how to relate the satellite-derived model to climate and terrestrial phenomena (15, 16). However, there is little doubt that the NDVI provides a useful space perspective monitor of vegetation, land cover, and climate, if used carefully. The index has been produced and utilized globally (6) and regionally (16–20).

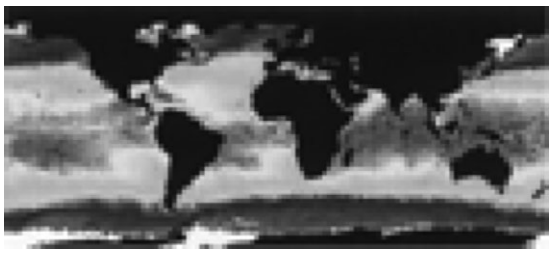

Figure 12. Sea surface temperature (°C) from infrared AVHRR data.

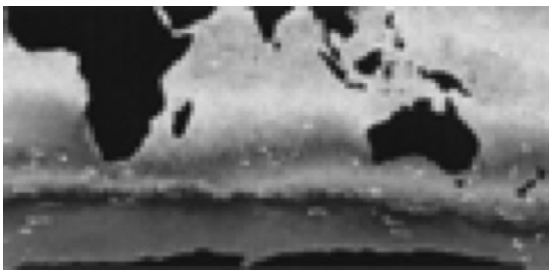

Figure 13. SST for May 1986 from the AVHRR with coincident buoy tracks (white).

Thermal Infrared Applications

Sea Surface Temperature (SST). Initially, thermal infrared imagery was collected to provide information on the atmosphere when the Earth was not in sunlight. Later it became clear that there were many nonmeteorological applications of these thermal infrared images. One well-known application is the computation of sea surface temperature. Traditionally computed from the reports of ships at sea and later autonomous drifting buoys, the satellite infrared data provided a substantial increase in the area covered for any specific time. Cloud cover was still a major problem because it obscured the infrared signal from the ocean. In addition, atmospheric moisture in the form of water vapor significantly altered the SST signal. In spite of these limitations, the satellite SST data were such a large increase in the time/space coverage of SST measurements that they completely changed the way SST was routinely calculated. Prior to the advent of satellite data, the SST measurements were limited to the major shipping routes and the limited areas where drifting buoys were deployed. Later the distribution of buoy data increased, and they became a major source of in situ SST data that was used to "calibrate" the thermal infrared satellite SST data. In this calibration, the buoy data are used as "ground truth," and the satellite SST algorithm is adjusted to fit the buoy in situ SST measurement.

Even with the satellite, SST data global fields are not usually full on a daily basis, and a compositing procedure is needed to create a global SST map (Fig. 12). This is a two-week composite of the Multi-Channel (MC) SST (21) with a 40 km spatial resolution. The satellite data used to generate this SST map were the 4 km spatial resolution Global Area Coverage from the NOAA AVHRR. Each image was first navigated to locate the pixels accurately. Clouds have then been filtered from each of the individual scenes used in the composite. In computing the composite SST, a maximum temperature has been retained because residual clouds will always lower the temperatures. This is much the same logic as is used with the maximum NDVI composite. The resultant field has further been smoothed by a Laplacian filter to reduce any noise in the spatial signal.

Notice the white patches that indicate cloud cover even after the compositing procedure. The striped appearance of Hudson Bay is due to an error in the smoothing program. The main features of the SST field are the tropical core of high SST, the coldest temperatures in the Polar Regions, and the highly variable regions at the boundaries of these fields. In the tropics, much of the spatial variability caused by waves propagating in the equatorial waveguide. It is notable that strong warm currents such as the Kuroshio and Gulf Stream are not readily apparent as patches of warm SST. This is likely the result of low spatial resolution and the Laplacian smoothing. The strong western boundary currents have simply been smoothed out of the map.

It is difficult to judge just how much credibility to give to individual features. One would like to say something about various current systems, but most known currents do not appear on this map. Furthermore, heating and cooling can have very dramatic effects, particularly on the tropical warm SSTs. In the southern polar region, it is tempting to suggest that the dark blue band represents the polar front with its meanders and eddy formation. Still in Fig. 9 this dark blue band extends much farther north than is usually thought to be the case for the polar front. Another suggestion of the expression of ocean currents by the SST pattern in the southern ocean can be seen in Fig. 13 where a month-long satellite SST similar to that in Fig. 12 has been computed and the coincident tracks of drifting buoys have been superimposed.

Note how well the buoys appear to follow the SST isotherms, particularly in the area around Cape Horn and into the Indian Ocean. Buoy trajectories just north of the light-blue area exhibit north and south excursions that are matched by the frontal features in the SST map. Because these are regions occupied by the Antarctic Circumpolar Current (*ACC*), it is realistic to have these apparently large velocities in the area. These fronts are known to be locations of strong currents that together make up the ACC. This is also the case south of the Australian bight where the buoy tracks now appear to follow the Subantarctic Front to the south of the light blue band. The continuation of strong currents is emphasized by the long trajectories for this monthly period. This is particularly apparent when these trajectories are compared with the monthly trajectories located to the north of the light-blue area.

Comparing the buoy locations also emphasizes that the coverage by drifting buoys alone is meager and that any SST made without the satellite data would be forced to interpolate between widely separated data points. For this particular comparison, it should be noted that there was a specific program to drop buoys in the southern ocean. When ship tracks are added, the data coverage increases, but then only along shipping routes. There are many areas that a ship does not visit nor are there usually any drifting buoy measured SSTs. Thus satellite data must be used to

compute a global SST with any hope for decent coverage.

There are many problems involved with combining infrared satellite SSTs with in situ measured SSTs. In situ measurement of SST is not a simple task, and there is the potential that errors exist both in archived in situ SSTs and in satellite SST ground-truthing procedures using in situ SST. Heating or cooling of the sea surface occurs as a result of the air-sea fluxes, horizontal and vertical heat advection, and mixing within the ocean. It is the nature of the air-sea fluxes of heat to complicate the measurement of SST in the ocean. The heat exchange associated with three of the four components of the net heat flux—the sensible heat flux, the latent heat flux, and the longwave heat flux—occurs at the air-sea interface. The heat exchange associated with the fourth component—the shortwave radiation—occurs over the upper few tens of meters of the water column. Typically, the sum of the three surface fluxes is negative (the ocean gives heat to the atmosphere), and the sea surface is cooled relative to temperatures just a few millimeters below the surface.

During daylight hours, the shortwave radiation penetrates and warms the water where it is absorbed. The absorption is an exponential function of depth, and the energetic red light is absorbed more rapidly (e-folding depth of approximately 3 m) than the less energetic blue-green light (e-folding depth of roughly 15 m), with the exact rate of absorption at each frequency depending on water clarity. Heating caused by solar insolation can produce a shallow, warm, near-surface layer meters to tens of meters in thickness. The surface is still cooled by evaporation, longwave radiation, and sensible heat flux; but the "cooler" surface temperature can, because it is the surface of the layer warmed by the sun, be greater than a temperature from below a shallow diurnal mixed layer [Fig. 14(a)]. During the day, the strong vertical temperature gradients within and at the base of the region that experiences diurnal warming make the measurement of sea surface temperature from engine intakes, temperature sensors attached to buoys, and other fixed-depth instruments difficult. At night, this shallow warm layer cools, and the continued surface cooling results in a skin temperature below that a few centimeters deeper [Fig. 14(b)]. As discussed in Schlüssel et al. (22), the difference between the skin SST and the bulk SST, 2 m below the surface, ranges from -1.0°C to 1.0°C over a 6-week period with a mean difference of 0.1°C to 0.2°C (positive values indicate a cool skin temperature).

Attempts to make in situ measurements of SST fall into two classes. Traditionally measurements have been made from ships with "bucket samplers." These buckets sample a temperature in the upper meter of the ocean. Because of its ease of operation, shipboard SST measurements shifted to the reporting of "ship-injection" cooling water temperature collected from intakes ranging from 1 m to 5 m below the sea surface. A study by Saur (23) indicated that heating in the engine room resulted in a bias of about $+1.5^{\circ}$C in these injection temperatures. Such problems with ship SSTs have led many people to the exclusive use of SST data from moored and drifting buoys. These systems sample temperature at a wide variety of depths ranging from 0.5 m to 1.5 m, depending on the hull shape and behavior in the wave field. Moored buoys with large reserve buoyancy

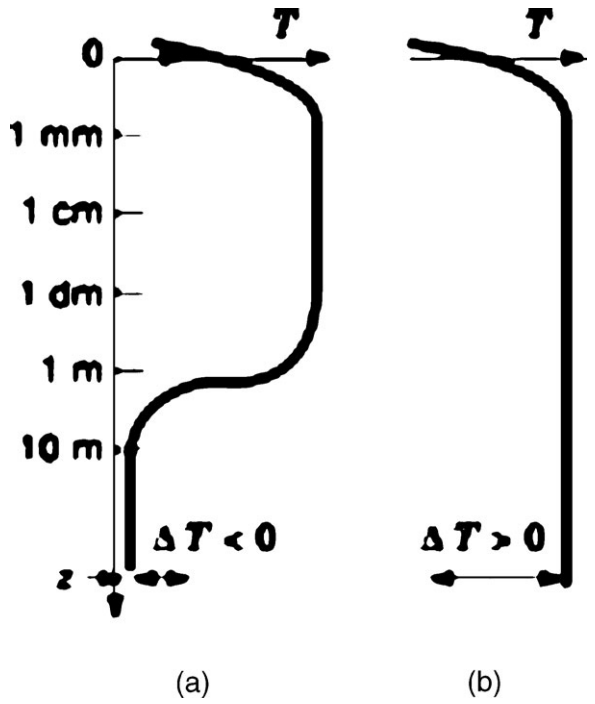

Figure 14. Ideal near-surface temperature profiles.

do not oscillate as much vertically as do the drifting buoys, which are often designed to minimize wind drag. Moored buoys provide temperature time series at a point, but the buoy does move up and down as it travels within its "watch circle."

All these in situ SST measurements sample a near-surface temperature that is commonly referred to as the bulk SST. This bulk SST has been used in the common "bulk formulas" for the computation of the surface fluxes of heat and moisture. Depending on the surface wind and wave and solar heating conditions, the bulk temperature differs greatly from the skin SST. It is the temperature of this thin molecular boundary layer (24) that radiates out and can be detected by infrared sensors. The sharp temperature gradient (Fig. 12) in this molecular sublayer is always present at surface wind speeds up to 10 m/s (25). At higher wind speeds, the skin layer is destroyed by breaking waves. Earlier studies (25, 26) have shown, however, that the skin layer reestablishes itself within 10 s to 12 s after the cessation of the destructive force.

Direct measurement of the skin temperature is not possible because any intrusion will destroy the molecular layer. Even drifting buoys cannot measure the temperature of this radiative skin layer because contact with the skin will destroy it for the duration of the contact. Ship-mounted infrared radiometers have been used (22, 27) to observe the ocean's skin temperature without the effects of atmospheric SST signal attenuation that are suffered by satellite-borne infrared sensors. In order to overcome the many errors inherent in this type of measurement, a reference bucket calibration system was developed. In this system, the bucket is continuously refreshed with sea water so as to ensure that no skin layer develops. The temperature of the reference bucket is continuously monitored,

and the radiometer alternately views the sea surface and the bucket, providing regular calibration of the radiometer. This calibration not only includes an absolute reference to overcome any drift of the radiometer blackbody references or instrument electronics but also will provide a calibration of the radiometer for the effects of the nonblackness of the sea surface, the contributions of reflected radiation from sky and clouds, and the possible contamination of the entrance optics by sea spray. Monitoring the bucket temperatures with platinum resistance thermometers, accurate to 0.0125°C, made it possible to measure the skin temperatures accurate to 0.05°C.

Other investigators (28) have relied on internal reference temperatures for the calibration of the skin SST radiometer using pre- and post-cruise calibrations to ensure the lack of drift in the reference values. To account for the nonblackness of the sea surface and reflected sky radiation, the radiometer was periodically turned to point skyward during variety of conditions. The resulting correction was an increase in the measured radiometric SST by an average of 0.25°C. This rather large average value emphasizes the need for a continuous reference calibrator for the ship skin radiometer measurements of SST.

All previously used radiometers have employed a single channel. Because the satellite radiometers that these ship measurements are designed to calibrate have more than a single channel, it would be useful if the shipborne radiometer also had multiple thermal infrared channels. Unlike the satellite measurements, where these different thermal channels are intended to be used for atmospheric water vapor attenuation correction, the multichannel shipboard radiometer would provide redundant measures of the emitted surface radiation and a better source of calibration information for the satellite SST.

Sea Surface Temperature Patterns. Some applications of satellite SST estimates do not involve the need for computing the precise SST, but rather it is the SST pattern that is important not the SST magnitude. Much as was seen in Fig. 8 where the drifting buoy trajectories matched the shapes of the temperature contours, the pattern indicates the current structure that we are interested in. This is most clearly the case for a western boundary current such as the Gulf Stream (Fig. 15) where the dark red indicates the core of the current that splits off into meanders and then eddies. In this image, we see three cold eddies that have separated from the Gulf Stream. The westernmost two are clearly still part of the Gulf Stream, but the eddy to the east appears to have separated as marked by the colder (green) center. Note the meander to the northwest where colder slope-water has been entrained from the north. This is the source water of the eddies that separate to the south.

Different studies have used the shape of the Gulf Stream core to estimate the long-term behavior of the current system. A line that separates the cold waters to the north from those of the Gulf Stream can be drawn. This is done every 2 weeks, and the resulting lines are then analyzed for the time/space character of the Gulf Stream. Other studies have examined the interaction between the eddies and coastal bottom topography. Warm rings that separate to the north eventually reach the continental shelf break where a strong upwelling that feeds the local fauna occurs. These warm eddies are known to be the locations of good fishing conditions, and some groups sell SST maps as a service to fishermen.

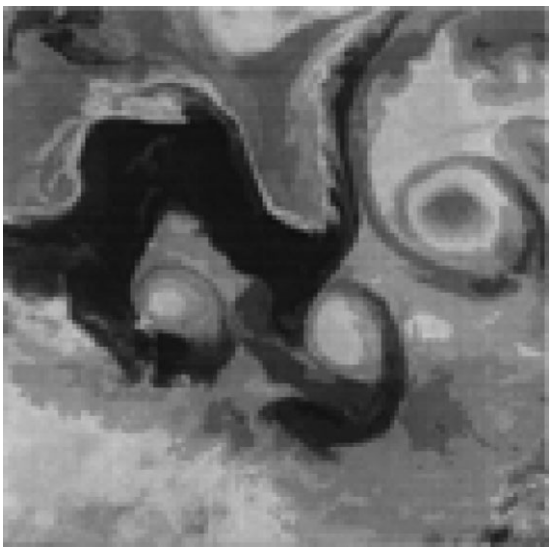

Figure 15. Sea surface temperature of the Gulf Stream region.

Combining Visible and Thermal Infrared Data

Snow Cover Estimation. The process of routinely estimating seasonal snow cover and converting it to snow water equivalence (*SWE*) for water resource management is currently labor intensive, expensive, and inaccurate because of the inability of in situ measurements to cover all the spatial variations in a large study area. It is attractive to use satellite data to monitor the snow cover because of the unique synoptic view of the satellite (29). If data from operational weather satellites can be used to estimate reliably annual snow pack and annual SWE, the seasonal snow pack assessments can be improved, and the water supply for the coming summer season can be better predicted. We introduce a new method for using satellite data from the Advanced Very High Resolution Radiometer to estimate the snow cover and the SWE from a series of images composited over time to remove cloud contamination. A pseudo-channel 6 is introduced that combines two AVHRR channels to discriminate snow from cloud objectively. Daily snow retrievals in individual AVHRR images are composited over one-week intervals to produce a clear image of the snow cover for that week.

This technique to produce snow cover maps routinely from AVHRR imagery is different from that used operationally (30). Our April 1990 snow cover was based on a composite of 7 to 14 different images, whereas the operational estimates are derived from a relatively limited number of AVHRR images.

A key to estimating SWE from a snow cover map derived from satellite data is a knowledge of the relationship between snow cover, snow depth, and the resultant SWE. A long (25 year) time series of historical snow pack measurements from Colorado SNOTEL and SNOW COURSE

sites was used to develop correlations between snow depth and elevation in the snow covered regions. It is well known (31) that above the tree line, or in areas where trees are so sparse that they provide little protection from the wind, there is no clear relationship between SWE and elevation. Instead, wind moves much of the snow after it falls, and other weather variables, like solar radiation, cause snow ablation to be larger in exposed areas. In most of the basins that we studied, less than 15% of the ground area is above tree line. Thus, we ignored this effect and assumed that SNOTEL and SNOW COURSE measurements provided good estimates of the snowpack at the elevations in each drainage basin.

Colorado was separated into seven river drainage basins, and the relationship between snow depth and elevation for each of these basins was calculated. The lowest correlations were not for those areas with the greatest elevations but rather for those areas with the poorest coverage in terms of ground measurement sites of snow depth. In one case, it was necessary to eliminate some sites in order to improve the correlations. These sites were located in the same region and were apparently not representative. The AVHRR snow cover maps were merged with a digital terrain map (*DTM*) of Colorado, and the snow elevations were computed from this merged set. Using linear regressions between snow depth and elevation from the historical data, these snow elevations were converted into SWE for each individual drainage basin. In each basin, river run-off was estimated from the gauged measurements of each river. There were large differences between individual basin gauge values (cumulated from all river gauges in the individual basins) and with the SWE estimates from the satellite and DTM data. These differences appeared to cancel out when the entire state was considered. There are transmountainal diversions, human-made tunnels used to divert water from one basin to another, that routinely shift water from one basin to another to satisfy demand. The only valid comparison was to lump the seven basins together and make an estimate for the state as a whole. This statewide estimate of SWE from the satellite imagery was found to be within 11.2% of the combined river run-off from the gauged rivers (taken from the maximum in 1990), when the first two weeks of April 1990 were used to make the composite image of snow coverage.

In order to determine how to use AVHRR data to assess winter snowpack conditions, it was necessary to decide when during the year such an assessment should be made. Because we are interested only in the long-term snowpack and not in the short-term transient snow, a long time series of snowpack measurements and multiple consecutive days of spatial snow coverage (from AVHRR) are considered. We analyzed 25 years of data from the US Department of Agriculture Soil Conservation Service (*SCS*) based on automated SNOTEL stations and manual SNOW COURSE stations across the state of Colorado. The SNOTEL stations measure snow depth by monitoring snow pillows, collapsible bags filled with antifreeze solution. The SNOW COURSE data are seasonal measurements of snow depth and water equivalence made manually over bimonthly intervals during the snow season. Each of the SNOTEL stations is manually verified once each year. While the SNOTEL measurements are recorded each day and are transmitted from these sites to a central location only on the first and fifteenth of each month. These values are published yearly in the Colorado Annual Data Summary, and digital values are available from the SCS West National Technical Center computer in Portland, Oregon.

The 25 years of SNOTEL data were averaged to find the mean annual SWE. The steplike character of this diagram reflects the fact that it is built from biweekly observations averages represented by the steps. There is a linear increase from October to the maximum at the beginning of April. After that there is a sharp decrease during the melt season of late May through July. We therefore selected the first part of April as the maximum snow extent and hence the time when we should estimate the annual snow cover from the AVHRR imagery.

Snow Cover from AVHRR Imagery.

Snow Image Calculation. The primary advantage of satellite imagery for snow mapping is the synoptic areal coverage provided by a single satellite image. This eliminates the changes over time and space that take place while collecting SNOW COURSE measurements. Satellite images also provide much greater spatial resolution than is possible even by combining SNOW COURSE measurements with automated SNOTEL sites. The disadvantage of the satellite imagery is the fact that snow and clouds appear similar in the visible and thermal infrared images. Both are bright reflective targets having very similar values in the AVHRR visible channel 1 (0.58 μm to 0.635 μm). Clouds and snow cover also have similar temperatures resulting in similar thermal infrared (channels 3, 4, and 5) signatures. To discriminate between cloud and snow, we introduce a fictitious channel 6 that is a combination of channels 3 (3.7 μm to 3.935 μm) and 4 (10.3 μm to 11.35 μm). We define channel 6 as

$$\text{Chan } 6 = (\text{Chan } 3 - \text{Chan } 4) \tag{2}$$

Because channel 3 contains both thermally emitted radiation and reflected radiation, the difference between channels 3 and 4 removes the thermal response portion from channel 3. In channel 6, clouds should appear much "brighter" than the snow pixels.

The channel 6 image is combined with the channel 1 visible image to determine clearly which areas of the visible image are clouds. Both clouds and snow are bright in channel 1 whereas clouds appear brighter than snow cover in the synthetic channel 6 image. Where bright values in channel 1 match with the bright features in the channel 6 image they are confirmed as cloud cover and masked out as such in the channel 1 image. The remaining bright values in channel 1 then represent the snow cover. This procedure is very different than the supervised classification procedure used by Baumgartner et al. (32) and Baumgartner (29). In this type of approach, it is possible to define "pure snow cover pixels" based on in situ measurements (33).

It is not possible to assess quantitatively the degree to which a "snow cover" pixel is occupied by snow, but we believe that the snow signatures in channels 1 and "6" indicate that the pixel is more than 75% snow covered. Most

of the pixels will be greater than that in snow cover with most of them at 100%. No in situ data were collected to analyze which of the snow pixels was 100% covered and which were less. This is an area for future study in order to better establish the accuracy of this type of remote sensing for mapping snow cover.

The procedure just described was used to create "snow images" for each day in the month of April 1990. In general, at least one AVHRR image per day was available for analysis. In some cases, there were two images (morning and afternoon satellite passes), and a correction was applied to account for differences in solar azimuth angles. Snow and clouds reflect light in the visible part of the spectrum. Radiation with wavelengths > 1.2 m is strongly absorbed by snow, and a snow-cloud discrimination channel centered at 1.6 m is planned for later versions of the AVHRR. In the thermal infrared, both snow and clouds absorb strongly in the range between 10 m and 12 m, but at 3.7 m clouds will reflect more light than snow. Hence the virtual channel 6 value will be greater for clouds. The problem that arises with high cirrus clouds is that they have a high ice crystal content and an albedo similar to snow. For this reason it was necessary to do some additional processing to further remove cloud residuals.

Cloud Residue Removal. After this mapping procedure was applied to each image, two different types of cloud versus snow discrimination errors remain. First, some snow pixels may have been mistakenly eliminated as clouds. Second, some clouds that have been improperly identified as snow will remain. These errors are partially accounted for by producing a composite image over time. Because clouds move over short time periods and snow changes more slowly over time, it is possible to retrieve those portions of individual images that are identified as snow and then composite them over a period of time. Thus bright features that change rapidly in time (between two images) are identified as clouds rather than snow even if they have passed the earlier filter process. In this way, we compensate for those image pixels that are clouds incorrectly identified as snow. Only those pixels that are identified as snow in more than one image are retained as snow cover.

This temporal composite has an additional benefit. Because we are interested in the snow cover that contributes to the annual basin run-off, we are not interested in the transient snow cover that may exist right after a snowfall. We are instead interested in the continuing seasonal snow cover that is found above the snowline (approximately 9,000 ft), which is the primary contributor to the spring water shed in Colorado. Our temporal image composites will eliminate the possible contribution from short-term transient snow cover.

Composite Snow Images. For our study week, long periods were used to composite the snow cover retrievals. Separate composite "snow images," as well as a composite image, were computed for the first and second weeks of April 1990. In these images, the bright white areas are the snow-covered regions and clearly depict the mountain ridges. The images seem to indicate a heavier snow cover for the first week than for the second week. This was caused by fresh snowfall early in the first week that then settled (melting, compacting, etc.) into snowpack in the second week. During this first week, the transient snow cover leads to a false estimate of the overall snowpack. The image for both weeks is likely to be more representative of the total snowpack as these transient conditions are smoothed out over this longer time period.

A technique was introduced to distinguish objectively between clouds and snow cover in multichannel AVHRR images. Introducing a pseudo-channel 6 as the difference between infrared channels 3 and 4, it was possible to discriminate snow cover from clouds by using channel 6 and the visible image of channel 1. Both clouds and snow cover appear bright in the visible channel, whereas clouds are darker in channel 6 so that it is possible to identify those portions of the channel 1 image that represent clouds. These are then masked off, and the remaining bright portions of the channel 1 image are determined to be snow cover.

Using a relationship between elevation and snow water equivalent developed for each major river basin from 25 years of historical in situ measurements, the satellite snow cover estimates for April 1990 were converted to a snow water equivalent. These values were then compared with the gauged values of river run-off and found to agree with 11% for the first two weeks of April when averaged over the entire state of Colorado. It was not possible to use this analysis for individual basins because water was diverted from one basin to another according to need. In addition, the individual weeks in April did not perform as well primarily because of a strong snowfall early in the first week.

These results suggest that it is possible to enhance snow cover assessments for Colorado using satellite remote sensing. Even though this approach will not replace the in situ measurements, it may be possible to reduce the number of expensive SNOW COURSE measurements or perhaps to improve the present snow pack assessments without any additional in situ measurements.

Ice Motion. It is possible to use a sequence of ice images to estimate ice motion. Here it is possible to use visible and infrared imagery in addition to passive microwave imagery that will not be discussed here. The basic requirement is to have excellent geolocation for each of the images. Any misregistration will result in an error in the estimated ice motion. For visible and infrared images, there is the usual requirement that the image be cloud free. This is something that almost never happens in Polar Regions where cloud cover is more prevalent than in other locations. Because of this extreme cloudiness, we use a different compositional technique. Instead of compositing the brightness values of the individual images, we composite only those areas that are clear enough to calculate the ice velocity vector. Thus we are now seeking areas that are clear in both the first and second image so that we can compute the ice velocity vector. We then composite the vectors from each pair of images over a period of time much as we did before for the individual images.

Ice motion can be clearly seen in the two images in Fig. 16, which are of the area between Greenland and Spitsber-

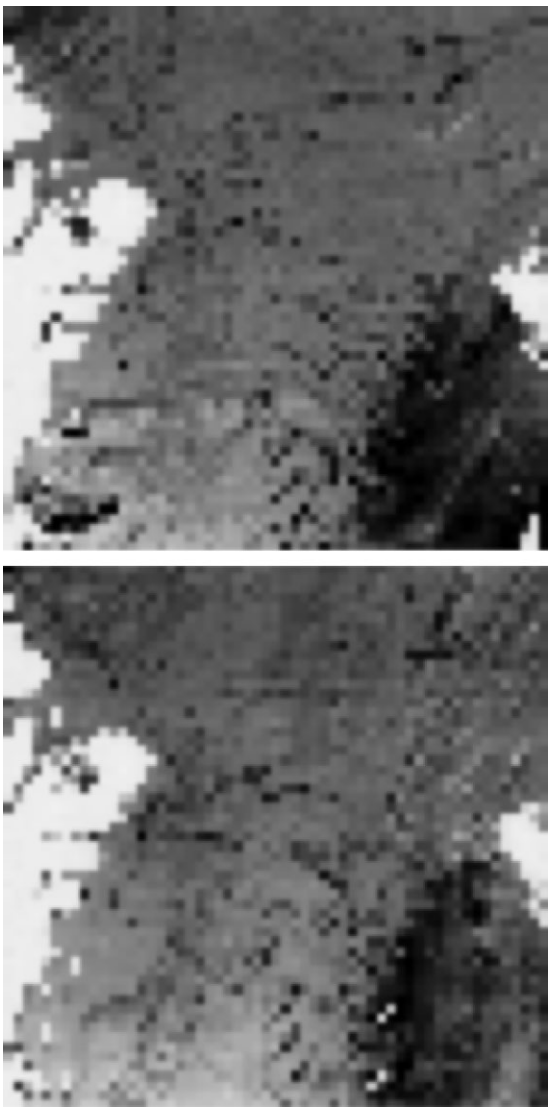

Figure 16. (a) Near-infrared image of sea ice in Fram Strait on April 21, 1986. (b) Near-infrared image of sea ice in Fram Strait on April 22, 1986.

gen known as Fram Strait. In this area, ice from the Arctic basic flows as in a funnel through this region, after which it continues to flow south. The strong shears present in this current regime are reflected in the very distorted images of the sea ice. We note that the clarity in terms of cloud cover is extremely unusual for these images and one cannot expect to view this area as clearly as this on any one occasion.

The technique used to detect the ice motion is the Maximum Cross Correlation (*MCC*) technique (34), which uses the cross correlation between the first and second images. To seek out the motion between the images, a large search window is used in the second images with a small "template" from the first image. The goal is to find the location at which the cross correlation between the template and search windows is a maximum. That then is the end of a velocity vector that reaches from the center of the search window to the center of the template window in this maximum correlation position. When search windows are overlapped, a densely populated velocity vector field is produced. This procedure can either be repeated for every image pair, or as above the clear portions of the images can be used to compute vectors that are themselves then composited to form a larger vector field. It is more attractive, however, to use the MCC approach to calculate the ice motion from the passive microwave images of the Special Sensor Microwave Imager (*SSM/I*), which has been done for both hemispheres by Emery et al. (35). Thanks to the lack of sensitivity of the passive microwave to atmospheric constituents such as water vapor, it is possible to view the ice surface regardless of cloud cover or the presence of atmospheric moisture. The only drawback is a decrease in spatial resolution going from 1 km with the AVHRR to a minimum of 12.5 km with the 85.5 GHz channel of the SSM/I. Lower-frequency SSM/I channels have a corresponding increase in resolution size up to about 25 km with the 37 GHz channel.

Forest Fire Detection and Monitoring

Another application that uses both the visible and thermal infrared channels is that of forest fire detection and monitoring. The vast area of most continents that is covered with forests requires constant observation to be able to spot fires when they first start and to deploy fire fighting men and equipment to control and put out the fires. A variety of systems are used today. They include ground-based electrical systems to detect lightening strikes that reach the ground along with observation towers built so that forest observers can see greater parts of the forest. These are supplemented with aerial surveillance, which also requires human observations. All these methods are manpower intensive and cannot possibly cover the entire area where forest fires occur. By comparison, satellite-based methods are or at least can be made fairly automated requiring human intervention mainly in the response to the site suspected to be on fire. Because of the potential for false fire identification, an additional confirmation is usually needed before resources will be deployed to fight the fire. It may be that, after considerable experience, it will be clear what satellite image signatures attend definite fires, reducing the number of fires that require additional confirmation.

There are two fundamental signatures of fires in weather satellite imagery. First is the "hot spot," which is the active fire itself (Fig. 17). This will be seen in the thermal infrared image as an extremely hot group of pixels. The fire must be a fairly large fire to fill the 1 km pixels of the AVHRR. The infrequent coverage of the SPOT and LANDSAT satellites does not make them optimum for rapid detection and monitoring. The frequent coverage of GOES is available only at the 1 km resolution in the visible channel, the lower resolution in the thermal infrared makes it impossible to map the hot spot unless it is greater than 4 km in size. One of the real problems in finding the hot spot is the fact that the smoke plume often obscures the actively burning part of the fire. But this smoke plume can also be used as a supplemental source of information on the fire itself. Here the problem is distinguishing the smoke plume from the ambient cloud cover. In the visible channel, the smoke and clouds look quite similar, and it is often

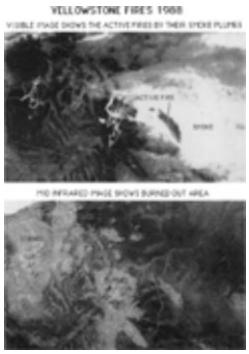

Figure 17. Thermal infrared (top) and 3.7 μm image (bottom) from the Yellowstone Fires 1988.

very difficult to discriminate between the two. The thermal infrared image provides some additional information because the cloud should be much colder than the smoke plume. Also the shape and position of the smoke plume can be used to infer something about the intensity of the fire and its position. All this information can be pooled to develop a description of the fire even before it is seen on the ground.

The major shortcoming of this approach is the need for more frequent coverage than is available from polar-orbiting sensors. With the present two-polar orbiter satellite system, it is only possible to view the fire every 4 to 6 h, which is enough time for the fire to really have changed its intensity, its direction, etc. GOES gives the required temporal resolution with its half-hourly imagery, but the problem is the lower spatial resolution in the thermal infrared channels. This is mostly the effect of sampling at a much higher altitude for GOES (22,000 km) as compared with ~800 km for the AVHRR. For the present, it is best to combine the visible GOES imagery with the AVHRR images to construct a more complete image of the fire and how it is progressing over time. This information can be used to augment (rather than replace) the ground-based fire detection and monitoring systems. In regions where there are no fire-monitoring stations, it may be that the satellite data are the primary sources of information for both detecting and monitoring the fire. Here they will guide the deployment of resources to fight the fire.

Although there is a lot of research that still needs to be done regarding the detection and monitoring of forest fires with satellite data, it is possible to construct a system that supplies the pertinent agencies with important information on the outset of the fires, their location and some selected information about fire intensity and progression in space/time. This system can be largely automated with no need for operator intervention until it comes to analyzing image features to evaluate the effect of cloud cover or perhaps to estimating which way the fire will progress. This is an important benefit of the satellite system when compared with any land-based system.

SUMMARY

There are a great many other applications of visible and infrared satellite imagery than those that have been presented in this article. In addition, new applications of these data are being discovered all the time, and it is impossible to stay abreast of the different processes being sensed by the satellite or at least being derived from the satellite data. One area of particular potential is merging the visible and infrared traditional satellite imagery with data from passive and active microwave sensors. These different bands are very complimentary with the microwave, offering all weather viewing at a substantially reduced spatial resolution. The optical channels, on the other hand, cannot provide uniform or comprehensive coverage because of cloud cover, but the temporal sampling is excellent. Thus we need to develop those indices that will take advantage of both types of data to yield new information about Earth's surface processes.

Another important research focus will be to find the best possible ways that satellite data can be integrated with model data. The assimilation of satellite data is a promising development in weather forecasting and should be equally as beneficial in studies of the Earth's surface. By merging models and satellite data, we are able to infer something about the fundamental processes influencing the Earth as sensed by the satellite.

BIBLIOGRAPHY

1. L. J. Allison E. A. Neil Final Report on the TIROS 1 Meteorological Satellite System, NASA Tech. Rep. R-131, Goddard Space Flight Center, Greenbelt, MD, 1962.
2. J. C. Barnes M. D. Smallwood *TIROS-N Series Direct Readout Services Users Guide*, Washington, DC: National Oceanic and Atmospheric Administration, 1982.
3. A. Schwalb The TIROS-N/NOAA A-G satellite series. NOAA Tech. Memo., NESS 95, NOAA Washington, DC, 1978.
4. A. Schwalb Modified version of the TIROS N/NOAA A-G Satellite Series (NOAA E-J)—Advanced TIROS N (ATN), NOAA Tech. Memo. NESS 116, Washington, DC, 1982.
5. ITT, AVHRR/2 Advanced Very High Resolution Radiometer Technical Description, prepared by ITT Aerospace/Optical Division, Ft. Wayne, IN, for NASA Goddard Space Flight Center, Greenbelt, Maryland 20771, under NASA Contract No. NAS5-26771, 1982.
6. K. B. Kidwell (ed.) *Global Vegetation Index Users Guide*, Washington, DC: NOAA/NESDIS/NCDC/SDSD, 1990.
7. M. Weaks LAC Scheduling; *Proc. North Amer. Polar Orbiter Users Group, 1st Meet.*, available from the NOAA National Geophysical Data Center, Boulder, CO, 1987, pp. 63–70.
8. G. R. Rosborough D. Baldwin W. J. Emery Precise AVHRR image navigation, *IEEE Geosc. Remote Sens.*, **32**: 644–657, 1994.
9. D. Baldwin W. J. Emery AVHRR image navigation, *Ann. Glaciology*, **17**: 414–420, 1993.
10. D. Baldwin W. Emery P. Cheeseman Higher resolution earth surface features from repeat moderate resolution satellite imagery, *IEEE Geosci. Remote Sens.* in press.
11. W. J. Emery M. Ikeda A comparison of geometric correction methods for AVHRR imagery, *Can. J. Remote Sens.*, **10**: 46–56, 1984.
12. F. M. Wong *A unified approach to the geometric rectification of remotely sensed imagery*, U. British Columbia, Tech. Rep. 84-6, 1984.

13. D. Ho A. Asem NOAA AVHRR image referencing, *Int. J. Remote Sens.*, **7**: 895–904, 1986.
14. L. Fusco K. Muirhead G. Tobiss Earthnet's coordination scheme for AVHRR data, *Int. J. Remote Sens.*, **10**: 625–636, 1989.
15. C. J. Tucker *et al.* Remote sensing of total dry matter accumulation in winter wheat, *Remote Sens. Environ.*, **13**: 461, 1981.
16. C. J. Tucker P. J. Sellers Satellite remote sensing of primary production, *Int. J. Remote Sens.*, **7**: 139, 1986.
17. C. J. Tucker *et al.* Satellite remote sensing of total herbaceous biomass production in the Senegalese Sahel: 1980–1984, *Remote Sens. Environ.*, **17**: 233–249, 1985.
18. S. N. Goward *et al.* Comparison of North and South American biomass from AVHRR observations, *GeocartoInternational*, **1**: 27–39, 1987.
19. S. N. Goward *et al.* Normalized difference vegetation index measurements from Advanced Very High Resolution Radiometer, *Remote Sens. Environ.*, **35**: 257–277, 1991.
20. C. Sakamoto *et al.* Application of NOAA polar orbiter data for operational agricultural assessment, *Proc. North Amer. NOAA Polar Orbiter Users Group 1st Meet.*, NOAA National Geophysical Data Center, Boulder, CO: 1987, pp. 134–160.
21. E. P. McClain W. G. Pichel C. C. Walton Comparative performance of AVHRR-based multichannel sea surface temperatures, *J. Geophys. Res.*, **90**: 11587–11601, 1985.
22. P. Schluessel *et al.* On the skin-bulk temperature difference and its impact on satellite remote sensing of sea surface temperature, *J. Geophys. Res.*, **95**: 13341–13356, 1990.
23. J. F. T. Saur A study of the quality of sea water temperatures reported in logs of ships weather observations, *J. Appl. Meteor.*, **2**, 417–425, 1963.
24. R. Saunders The temperature at the ocean-air interface, *J. Atmos. Sci.*, **24**: 269–273, 1967.
25. E. Clauss H. Hinzpeter J. Mueller-Glewe Messungen der Temperaturstruktur im Wasser an der Grenzflaeche Ozean-Atmosphäre, *Meteor Forschugsergeb., Reihe B.* **5**: 90–94, 1970.
26. G. Ewing E. D. McAlister On the thermal boundary layer of the ocean, *Science*, **131**: 1374–1376, 1960.
27. H. Grassl H. Hinzpeter *The cool skin of the ocean*, GATE Rep., 14, 1,pp. 229–236, WMO/ICSU, Geneva, 1975.
28. P. A. Coppin *et al.* Simultaneous observations of sea surface temperature in the western equatorial Pacific ocean by bulk, radiative and satellite methods. *J. Geophys. Res., suppl.*, **96**: 3401–3409, 1991.
29. M. F. Baumgartner Snow cover mapping and snowmelt runoff simulations on microcomputers, *Remote Sens. Earth's Environ., Proc. Summer School*, Alpbach, Austria, 1989.
30. T. R. Carroll *et al.* Operational mapping of snow cover in the United States and Canada using airborne and satellite data, *Proc. 1989 Int. Geosci. Remote Sens. Symp. 12th Canada. Symp. Remote Sens.*, Vancouver, B.C., Canada, 1989.
31. K. Elder J. Dozier J. Michaelsen Snow accumulation and distribution in an alpine watershed, *Water Resources Res.*, **27**: 1541–1552, 1991.
32. M. F. Baumgartner K. Seidel J. Martinec Toward snowmelt runoff forecast based on multisensor remote-sensing information, *IEEE Trans. Geosci. Remote Sens.*, **GE-25**: 746–750, 1987.
33. A. Rango Assessment of remote sensing input into hydrologic models, *Water Res. Bull.*, **21**: 423–432, 1985.
34. R. N. Ninnis W. J. Emery M. J. Collins Automated extraction of sea ice motion from AVHRR imagery, *J. Geophys. Res.*, **91**: 10725–10734, 1986.
35. W. J. Emery C. W. Fowler J. A. Maslanik Satellite derived Arctic and Antarctic Sea Ice Motions: 1988–1994, *Geophys. Res. Lett.*, **24**: 897–900, 1997. Links

WILLIAM J. EMERY
University of Colorado, Boulder, CO